

# An experimental study on a flat-plate-type solid propellant rocket motor

Masafumi Tanaka<sup>\*†</sup> and Katsuya Urakawa<sup>\*</sup>

<sup>\*</sup>National Defense Academy,  
Department of Aerospace Engineering, School of Systems Engineering,  
1-10-20, Hashirimizu, Yokosuka, Kanagawa 239-8686, JAPAN  
Phone : +81-46-841-3810 Ex.2581

<sup>†</sup>Corresponding address : tanaka@nda.ac.jp

Received : November 19, 2011 Accepted : February 22, 2012

## Abstract

Owing to no requirement for a propellant feed system, a solid rocket motor has a great advantage to design freely its configuration. A thin flat-plate-type motor was proposed. Upon the basis that the propellant mass was 10g and the diameter of end burning grain was 77 mm, the motor performance was investigated experimentally. Each component was shortened in the thrust direction. It was clarified that a sudden contraction of nozzle divergent section and a reduction of chamber free space disturbed the inlet flow to the nozzle and decreased the specific impulse. Multiple nozzles effectively shortened the motor thickness, but reduced the specific impulse furthermore. Experimental data of L instability at low pressure and the structural mass increment at high pressure enabled calculate an optimum thickness of the motor. Actually fabricated flat-plate-type motor worked well as a retro motor for a dropping pallet. However, scattering properties such as a pressure buildup delay indicated a difficulty for precise control of the motor behavior.

**Keywords** : solid rocket motor, propellant, rocket propulsion, pyrotechnics

---

---

## 1. Introduction

One of the distinguished advantages of a solid propellant rocket motor is a high degree of freedom for its geometric design. Thanks to no requirement for a propellant feed system, any configuration will be available. Another advantage of a solid rocket motor is a high thrust density, where the thrust density is defined as a ratio of the thrust divided by the face front area. A thin flat-plate-type configuration is a good example to demonstrate the advantages of the solid rocket motor. Recently unmanned aerial vehicles (UAVs) have been developed for a wide ranged operational fields<sup>1)</sup>. Not spoiling the aerofoil configuration, the small-sized flat-plate-type solid propellant rocket motor can be attached to a vehicle and be used as a retro motor for a safe landing or a swift maneuvering. When the motors are used as a set of multiple units, high thrust is available for decelerating a heavy payload.

The design concept of a thin flat-plate-type motor is very simple. Each structural component should be made compact axially. Since conventional solid rocket motors

have a cylindrical or spherical configuration, some problems will occur. The objectives of this study are to clarify the problems, to elucidate the effect of flattened motor configuration on the thrust performance, and to make a demonstration flight of a flat-plate-type rocket motor.

## 2. Design concept

A flat-plate-type solid propellant rocket motor consists of four main components; combustion chamber, propellant grain, igniter, and nozzle.

Compression in the axial length of the combustion chamber is achieved by reducing the axial free space as small as possible and by eliminating nozzle contraction part. Small free chamber space may induce so-called L instability.<sup>2)</sup> Rapid convergent flow may be disturbed in the flow pattern at the entrance to the throat, which will lead to non-isentropic expansion.<sup>3)</sup> From a point of view of the thermodynamics, the chamber pressure should be high. High chamber pressure in a flat vessel requires a structural consideration different from a conventional

rocket motor, since the internal pressure brings severe bending moment to the flat end plates, besides the tension stress to the side wall.

The constraint of the combustion chamber shape restricts the propellant grain geometry. To reduce the motor length, flat and thin grain configuration is practical. The whole grain surface should be ignited simultaneously and burned out at the same instance. The igniter should satisfy such a property.

In order to shorten the nozzle length, multiple nozzles are effective. On the condition that the chamber pressure and the nozzle expansion ratio are kept constant, the number of the nozzles decreases the nozzle size with keeping geometric similarity. When the number of nozzles is  $N$ , each throat area is inversely proportional to  $N$ , and the nozzle length is inversely proportional to the square root of  $N$ . It means that, when four nozzles are adopted, the nozzle length can be decreased to half. Downsizing of the nozzle makes the viscous flow effect not negligible. The gas flow pattern will be intricate without a nozzle contraction part. Narrow chamber free space and thin propellant grain may cause an unsteady and unsymmetrical character to the internal flow. It should be verified whether multiple nozzles produce unbalanced thrust or not.

**3. Experimental procedures**

Propellant used was a conventional composite propellant with 80% ammonium perchlorate and 20% hydroxyl-terminated polybutadiene in mass. The end-burning grain diameter was 77 mm and the web length was 1.3 mm. The propellant mass was around 10 g, of which value was selected to produce 20 Ns in total thrust. Three configurations of rocket motor were used to elucidate the effect of the flattened shape on the thrust performance and to make a demonstration of the flight motion. One was a conventional type, which had a gentle nozzle contraction section making the nozzle flow smoothly converge. The second was a flat type without nozzle contraction section, leading to a radially convergent flow. An experimental setup is shown in Figure 1. On a flat endplate on the exit side, the number of the nozzles was

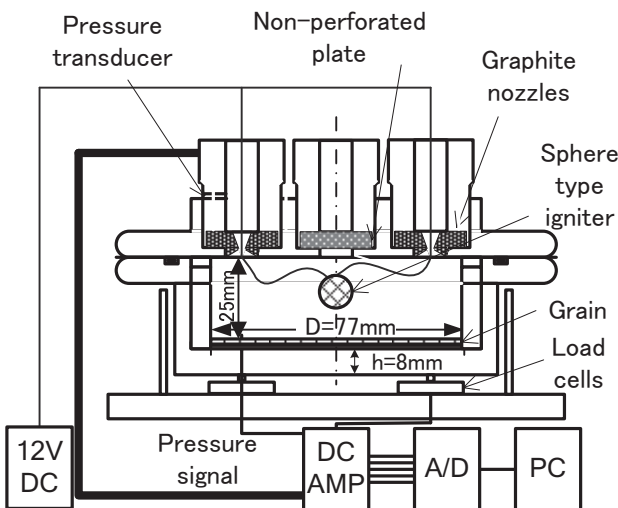


Figure 1 An experimental setup of a flat-type motor.



Figure 2 A picture of a thin-flat-plate motor for a demonstration flight.

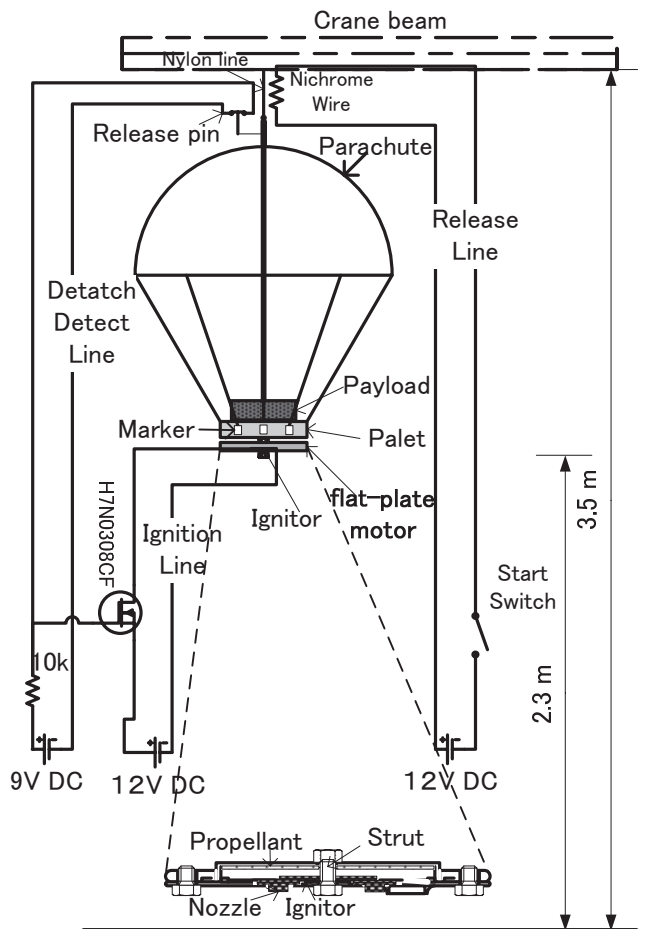


Figure 3 Schematic of a demonstration flight test.

variable from a single to four. Four load cells were set just under the multiple nozzles to measure the thrust balance. Both motor cases were able to change the chamber characteristic length  $L^*$  by inserting appropriately thick spacers behind the propellant grain.

The third was a thin-flat-plate motor which was used in the demonstration test. The demonstration flight was done with a small dropping pallet with a payload. A picture of the motor and a schematic of experimental setup are shown in Figures 2 and 3. More precise procedures will be described in the following section.



## 4. Results and discussions

### 4.1 Combustion chamber in flat shape

The effect of the elimination of the nozzle contraction section on the thrust performance was examined by comparing the conventional shaped motor and the flat one. The chamber characteristic length was adjusted to be the same between them. In this case the chamber free space was marginal enough to insert a spherical ignition powder. Typical pressure time histories are shown in Figure 4. It is seen that the flat type showed the progressive burning with a high peak pressure. Although the gas residence time was the same in both chambers, the ignition and the burning processes were not the same. The uniformity of the ignition was disturbed by the flat end plate. Moreover, the average pressure was high in the flat type motor. It is not well explained by the difference of the ignition phenomenon. The averaged thrust performances are shown in Table 1. Both specific impulses were low compared with the theoretical one around 230 sec. It was probably due to the motor down-sized effect and the short duration of the motor operation. In addition the graphite nozzle appeared to be not connected smoothly enough to the motor case inner wall. When the gas flow near the nozzle entrance was disturbed, the effective throat area would be decreased from the geometrical value. It can explain why in Table 1 high  $c^*$  efficiencies were attained in two type motors, where  $c^*$  means a characteristic velocity and  $c^*$  efficiency is defined as a ratio of experimental  $c^*$  to theoretical one. The reason why the  $c^*$  efficiency was extremely high, exceeding 100%, in the flat-type motor was ascribed to the acute curvature of the nozzle entrance. A two-dimensional effect appeared in the inlet

**Table 1** Comparison of thrust performance between a conventional motor and a flat-type one.

Type	Specific impulse $I_{sp}$ [s]	Characteristic velocity $c^*$ [m/s]	Thrust coefficient $c_F$	$c^*$ efficiency $\eta_{c^*}$ [%]
Conventional	171.0	1344	1.25	93.4
Flat-plate	180.9	1751	1.01	121.5

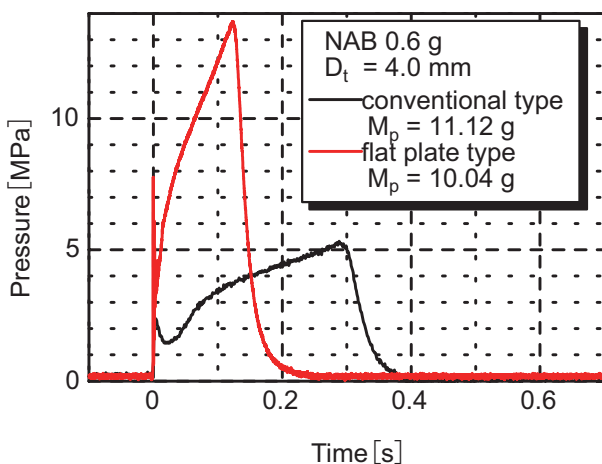


**Figure 4** Pressure time histories of a conventional motor and a flat-plate-type one.

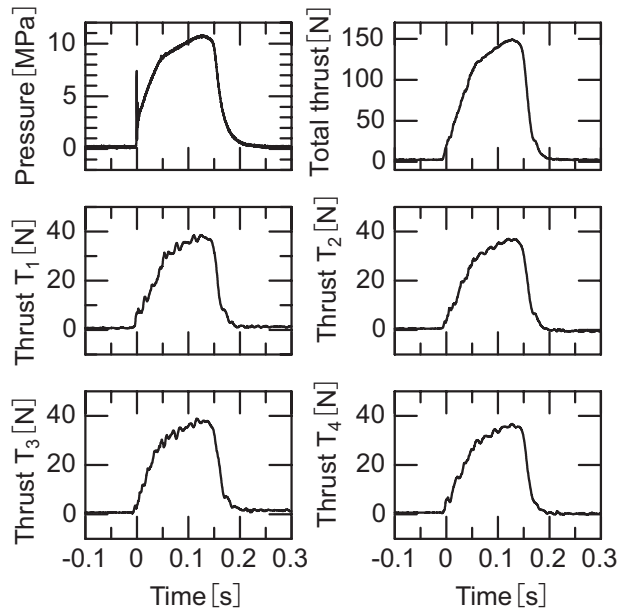


**Figure 5** Pressure and each thrust produced through multiple nozzles.

flow to the nozzle. It impeded smooth gas ejection and increased the chamber pressure. The conventional type presented lower specific impulse than the flat-plate type. It would be due to the low combustion pressure and an increment in heat loss to the exposed area of convergent section. The heat loss would reduce the chamber temperature and the characteristic velocity  $c^*$ .

### 4.2 Multiple nozzles

Multiple nozzles in the number of four were adopted to reduce the nozzle length. In order to examine whether the thrust unbalance appears, independent four load cells were set corresponding to each nozzle location. Figure 5 shows a typical example of the thrust time history. It is seen that the thrust unbalance did not appear.

### 4.3 Shortened chamber free space length

The effect of the reduction in the chamber free space on the thrust performance was investigated. Due to the narrow chamber free space, the igniter was changed from a sphere type to a sheet type to facilitate the entire surface ignition. Powder of boron/potassium nitrate was mixed with Viton in the ratio 8 to 2. They were dissolved into acetone and cured on a paper into a round sheet film. The volume of the chamber free space was changed, shortening the gap between the grain surface and the nozzle endplate with inserting a spacer behind the grain. Typical examples of the pressure time history are shown in Figure 6. Chamber free space gap length,  $L_c$ , was changed from 25 mm to 3 mm, of which value corresponds to 9.3 m to 1.1 m in  $L^*$ . The mass of the ignition powder was also varied. It is seen that the adoption of a sheet type igniter brought a neutral burning, by contrast with a progressive burning in Figure 4 in the case that  $L_c$  was 25 mm with a sphere type igniter. When  $L_c$  was 15 mm, even the sheet type igniter induced the peak over pressure after the ignition. The reduction of the ignition powder

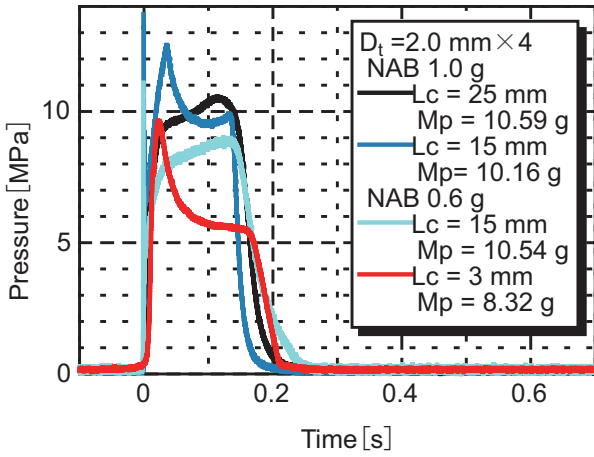


Figure 6 Pressure time histories of various chamber free space gaps,  $L_c$ .

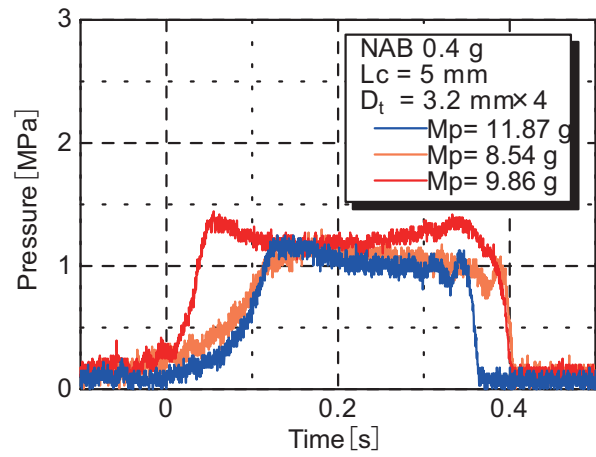


Figure 8 Pressure time histories in low pressure operation.

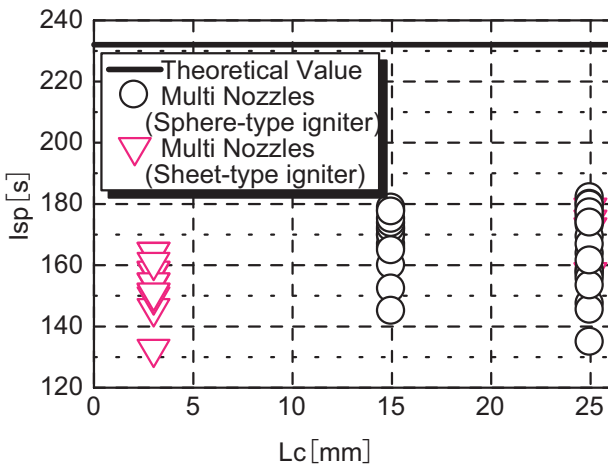


Figure 7 Specific impulse of various chamber free space gaps,  $L_c$ .

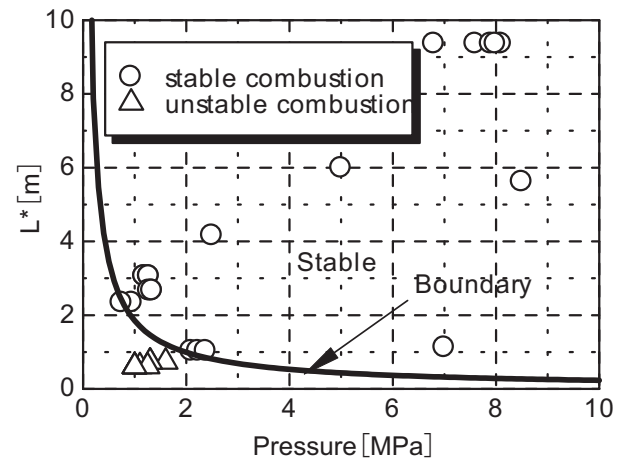


Figure 9  $L^*$  vs. pressure for conditional stability.

mass from 1.0 g to 0.6 g was effective to neutralize the pressure history. In the case that  $L_c=3$  mm, the mass of 0.6 g was excessive, although the averaged pressure was decreased due to the low total propellant mass.

The relation between the chamber free space gap  $L_c$  and the specific impulse was shown in Figure 7. As described before, experimental specific impulse was low by more than 20% of the theoretical value. The lower the chamber space length became, the lower the specific impulse was. According to a decrease in  $L^*$ , experimental  $c^*$  was decreased (the data are not shown here for saving the space). Insufficient combustion effect can explain the decrement in specific impulse in thinner chamber free space.

### 4.3 Low pressure operation and optimum motor total thickness

From a point of view of thermodynamics and chemical reactions, high combustion pressure is desirable to obtain the high thrust performance. On the other hand, high pressure is followed by heavy structure mass and it decreases the mass ratio of the vehicle. When the throat area is wide, the combustion chamber becomes low and the structure mass is reduced. Although in theoretical calculation a decrease in pressure does not reduce the

specific impulse so much, excessively low pressure induces so called  $L^*$  instability. Low pressure operation was investigated. Typical results are shown in Figure 8. In the figure, since high frequency noise filter was released to detect whether high frequency instability occurs, the curves included severe white noise. It is seen that at low pressure and in low  $L^*$  condition, low frequency oscillations appeared, but high frequency instability was not observed.  $L^*$  oscillation has been explained by a comparable situation between the chamber residential time and the burning combustion response delay. To avoid  $L^*$  oscillation the next condition should be satisfied :

$$L^* \geq \alpha p_c^{-2n} \tag{1}$$

where  $n$  is pressure exponent of the propellant and  $\alpha$  is a constant to be determined by an experiment.<sup>4)</sup> Changing  $L^*$ , stability condition was obtained as Figure 9. The stable region and the unstable region were divided by the boundary as Eq. (1), where  $\alpha$  was determined as  $8.33 \text{ m/MPa}^{-2n}$ .

Based on a simple calculation, the effect of the motor total thickness on the velocity increment of a vehicle was examined. The total thickness of the rocket motor consists of the chamber free space gap, two motor endplate thicknesses (motor head side and nozzle side), propellant



web length, and nozzle length. The last two terms can be constant. The motor endplate thickness,  $h$ , is calculated, assuming the safety factor to be 1.0, as

$$h = \sqrt{\frac{3p_c D}{4\sigma_{max} 2}} \quad (2)$$

where  $D$  is the chamber diameter, and  $\sigma_{max}$  the yielding stress.<sup>5)</sup> The chamber space gap is determined by the minimum  $L^*$  value in Eq. (1). The masses of the structure and the propellant determine the velocity increment  $\Delta V$  of the vehicle as

$$\Delta V = I_{sp} g_0 \ln MR \quad (3)$$

where  $I_{sp}$  is specific impulse calculated by theoretical CEA code,<sup>6)</sup>  $g_0$  standard gravity constant, and  $MR$  mass ratio. Let us assume a cylindrical motor case with an inner diameter  $D$  assembled from two endplates and a side wall of  $h$  in each thickness. When the mass of the nozzle parts is negligible and the vehicle has no payload, the motor dry mass  $M_B$  and the mass ratio are calculated as

$$M_B = \left\{ \frac{\pi}{2} D^2 h + \pi (D + h) h L \right\} \rho_m \quad (4)$$

$$MR = (M_B + M_p) / M_B \quad (5)$$

where  $M_p$  is the propellant mass,  $L$  the height of the motor case inner space, and  $\rho_m$  the density of the case material. The inner height  $L$  should be determined from the propellant web length and the chamber free space gap.

Assuming that the motor includes 10 g propellant of 125 mm in diameter and the motor case consists of a titanium alloy of  $\sigma_{max}$  920 MPa and density 4400 kg/m<sup>3</sup>, the relation between the velocity increment and the motor thickness was obtained as Figure 10. Theoretically the minimum thickness of 8.96 mm appeared around 10 MPa, although the highest velocity increment was obtained in 16 mm thickness at the chamber pressure 3 MPa. When the pressure was low, marginal chamber free space was needed to avoid  $L^*$  instability. It increased the motor total thickness and the corresponding increment in the motor mass reduced  $\Delta V$ . On the contrary, when the pressure was high, there was no need for a marginal free space, but

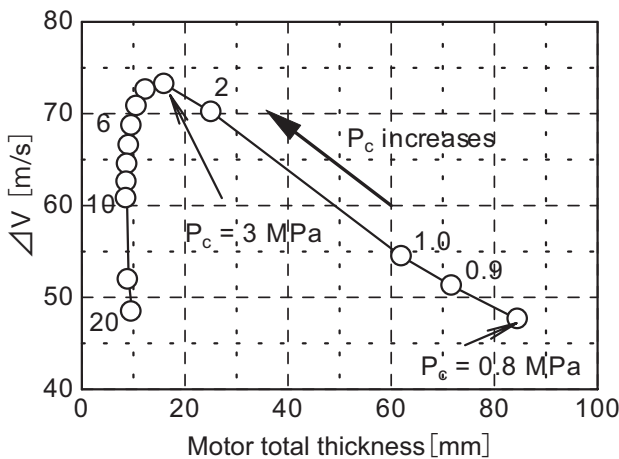


Figure 10 Relation between velocity increment and motor total thickness.

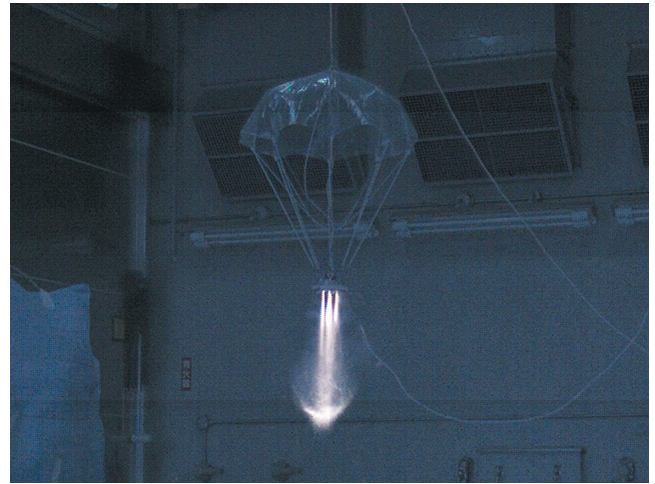


Figure 11 Demonstration flight of a flat-plate-type motor.

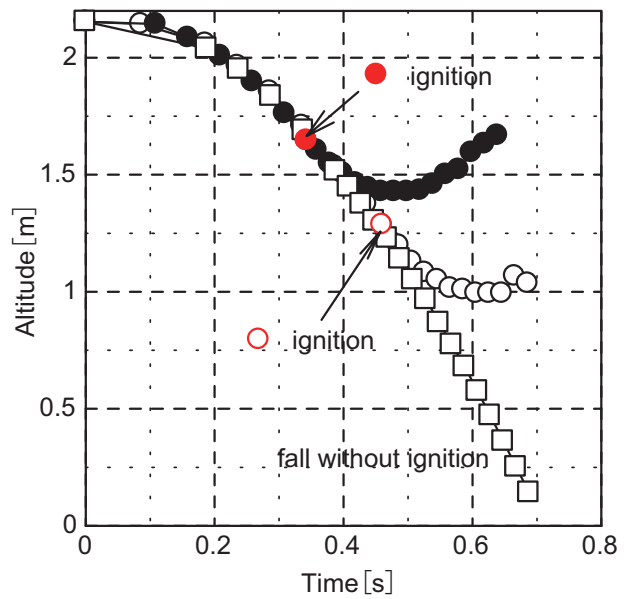


Figure 12 Motor ignition and trajectories of the dropping pallet.

the endplates and the side wall should be reinforced in thickness. The increased mass decreased  $\Delta V$ . Maximum  $\Delta V$  appeared at 3 MPa.

#### 4.4 Demonstration flight of a flat-plate-type motor

The purpose of the demonstration flight was to visualize the operation of the motor and illuminate the practical problems. Due to a financial restriction the motor case consisted of stainless steel (SUS304) in total thickness of 13 mm. The motor had four nozzles. Each throat diameter was 2.7 mm, and the chamber pressure was set 2 MPa in average. An ignition lag should be clarified in advance to control the dropping pallet. In this experiment we defined a pressure buildup lag as the time lag from the input of the ignition signal to the time when the pressure reached 0.3 MPa. Ten times ground static tests showed that the pressure buildup lag was 0.63 s in average having a standard deviation of 0.125 s. The ignition timing was set, intending the velocity to be zero at a 50 cm altitude. The parachute was used to keep the dropping pallet in a horizontal plane at the starting moment. The trajectories

of five drop tests, including one without ignition, were analyzed in motion pictures of a high speed camera. A picture of the dropping pallet is shown in Figure 11. Typical three relations between the altitude and the collapsed time are shown in Figure 12, where the ignition input signals were shown as arrow marks. The motor failed to kill the speed completely in four trials, and sometimes lifted the pallet. However, during the motor operation, the pallet kept its level. Although the effectiveness of multiple nozzles was well confirmed, the flight tests also indicated that scattering properties of the pressure buildup lag, the propellant mass, and the burning process in the motor are crucial factors to control the descending speed.

## 5. Conclusions

Shortening each component of a solid rocket motor axially, a compact thin flat-plate-type was realized. An elimination of the convergent nozzle contraction section and a reduction of chamber free space gap made the specific impulse low by 20% from the theoretical value. Although the characteristic velocity appeared to exceed 100%, the disturbance of the inlet flow to the nozzle decreased the specific impulse. Adoption of multiple nozzles was effective to reduce the motor thickness. Although it did not induce an unbalanced thrust, it decreased the specific impulse furthermore. A sheet type

igniter enabled a neutral burning. Low pressure operation caused L\* instability and high pressure operation needs an increment in structure mass. Optimum thickness was calculated theoretically. Actual flat-plate-type motor was fabricated and demonstrated well the function of retrorocket, decreasing a dropping pallet speed. Scattering properties such as a pressure buildup lag, etc. are critical factors to decelerate the speed and control the motor altitude.

## References

- 1) L. R. Newcome, "Unmanned Aviation: A Brief History of Unmanned Aerial Vehicles," AIAA, Inc. (2004).
- 2) E. W. Price, "Experimental Observation of Combustion Instability," Progress in Astronautics and Aeronautics Vol. 90, pp.733-790 (1984).
- 3) D. K. Huzel and D. H. Huang, "Modern Engineering for Design of Liquid-Propellant Rocket Engines," pp.73, AIAA, Inc. (1992).
- 4) M. W. Beckstead and E. W. Price, AIAA Journal, 5, 1989 (1967).
- 5) Y. Takeuchi, "Zairyo-rikigaku," pp.290, Nisshin-Shuppan (1969)
- 6) S. Gordon and B. J. McBride, "Computer Program for Calculation of Complex Chemical Equilibrium Composition and Applications," NASA Reference Publication 1311 (1994), <http://www.grc.nasa.gov/WWW/CEAWeb/>. (accessed: 14-Nov.-2011) (online).

# 薄型固体ロケットモータに関する実験的研究

田中雅文\*†, 浦川克也\*

推進薬供給系を考慮せずすむ固体ロケットモータは設計上, 自由な形状が採れるという大きな利点がある。薄型の板状モータを提案した。推進薬質量10g, グレイン直径77mmの制約の基に推進性能を実験的に調べた。各要素を推力方向に短くして性能を検討した。急激なノズル収縮部と狭い燃焼室空間が比推力を低下させる。マルチノズルは有効であるが, さらに比推力を低下させる。低圧で発生したL\*振動のデータと高圧での構造質量の制約から最適なモータ厚さを求めることができた。実際に作製したモータは降下パレットの減速に成功した。しかしながら, 圧力立ち上がり遅れ等の散在的化した現象がモータ運動の正確な制御を阻むことも示された。

\*防衛大学校

〒239-8686 神奈川県横須賀市走水1-10-20 システム工学群航空宇宙工学科

Phone: 046-841-3810内2581

†Corresponding address: tanaka@nda.ac.jp